Photoelectron angular distribution of atoms in pulsed XUV and IR fields

Xiao-Min Tong*
Center for Computational Sciences, University of Tsukuba, 1-1-1 Tennodai, Tsukuba, Ibaraki 305-8573, Japan

(Received 2 September 2018; published 24 April 2019)

We investigate theoretically the photoelectron angular distribution of atoms in pulsed XUV and IR laser fields by solving the time-dependent Schrödinger equation and surprisingly find that the angular distributions of sidebands are not always straight lines (normal) in the energy-angle plot as predicted by the strong-field approximation. Comparing our results with those of the strong-field approximation, in which photoelectron nucleus Coulomb interaction is ignored, the bending of the angular distribution is attributed to the photoelectron-nucleus Coulomb interaction. The bending depends on the IR intensity, IR pulse duration, XUV photon energy, and the time delay between the two pulses.

DOI: 10.1103/PhysRevA.99.043422

I. INTRODUCTION

The combination of an extreme ultraviolet (XUV) source generated from high-order-harmonic generation (HHG) [1,2] and the driving infrared (IR) laser presents an opportunity to investigate and control atomic photoabsorption processes. Several sidebands as predicted in theory [3] have been observed in experiments [4,5]. If short XUV and IR pulses are used, the strengths of the sidebands can be controlled by the time delay between the two pulses [6,7].

The mechanism of the IR-assisted photoabsorption can be explained as follows: The energy structures of an atom in an IR field are described by Floquet states [8], a Floquet state has many sidebands separated by one IR photon energy, and an electron can be ionized or excited by an XUV to a Floquet state through different sidebands, or different paths. Therefore, the energy distributions of photoelectron are also separated by one IR photon energy (sideband structure) and the sideband yields are sensitive to the relative phase or arriving time between the XUV and IR pulses [9,10]. Therefore, one can control the sideband yields by steering the time delay between the two pulses. Meanwhile, if one can control the relative strengths of the HHGs, one can also control the XUV photoabsorption cross section as predicted in theory [11] and confirmed by experiment [12].

Different from the XUV source generated from HHG, which is of the form of an attosecond pulse train (APT) [13,14] or a single attosecond pulse (SAP) [15,16], the photon energy of the XUV source radiated from a free-electron laser [17] can be tuned almost continuously and the pulse width can be narrowed in a femtosecond timescale, so it opens another dimension to study the IR-assisted photoabsorption process as recently reported in both theories [18,19] and experiments [20,21]. The two experiments focused on the photoelectron angular distribution.

When we investigated the photoelectron angular distribution of Ar atoms ionized by an XUV assisted with IR fields as reported recently in two experiments [20,21], we surprisingly found that the sideband angular distributions are not isoenergy separated by one IR photon energy or straight lines in energy-angle plots as predicted by the strong-field approximation (SFA) [22–25] if we use a lower XUV photon energy. We define this non-straight-line distribution as bending of a photoelectron angular distribution or simply bending in the following discussion.

To investigate the origin of the bending of a photoelectron angular distribution and simplify the problem, we simulated the photoelectron angular distribution of H atoms in two-color XUV and IR laser pulses and confirmed that the angular distribution is not always isoenergetic. Simply switching off the photoelectron nucleus Coulomb interaction in the simulation, the SFA does predict isoenergy distributions as shown in Fig. 1, which are consistent with our present knowledge of the angular distribution for multiphoton absorption. This clearly shows that the bending is attributed to the Coulomb effect, which is ignored in the SFA.

In this work we systematically investigate how the bending depends on the IR intensity, pulse duration, and the time delay between the two pulses. Since we focus on the IR-laser-assisted photoelectric effect, we assume that the IR pulse is longer than the XUV pulse and both pulses are longer than one period of the IR laser in this paper.

II. THEORETICAL METHOD

The atomic photoabsorption by an XUV light in an IR field can be studied by solving the time-dependent Schrödinger equation (TDSE) numerically. The detailed method has been published [26], so we only provide the key working equations for later discussion. To compare with the SFA, we solve the TDSE in the integral form [27,28]. All the dynamical information can be obtained from the equation [27] (atomic units $\hbar = e = m_e = 1$ are used hereafter unless stated otherwise)

$$\Psi(t) = -i\int_{-\infty}^{t} T\left[\exp\left(-i\int_{t''}^{t} H(t')dt'\right)\right] V_{\mathrm{XUV}}(t'') \times e^{-iH_0 t''}\Psi_0 dt'' + e^{-iH_0 t}\Psi_0. \quad (1)$$

*tong.xiaomin.ga@u.tsukuba.ac.jp

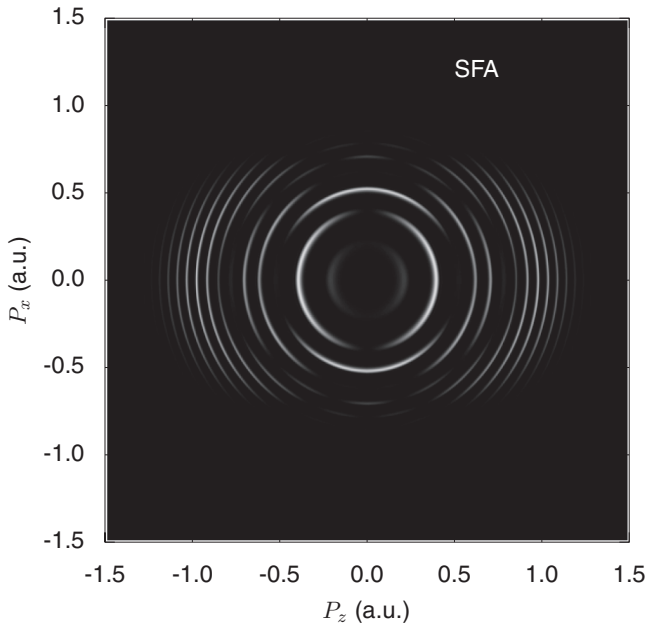

FIG. 1. Photoelectron momentum distribution of H atoms ionized by an XUV light in an IR field calculated by the SFA. The IR laser intensity is $2 \times 10^{13}\mathrm{W/cm^2}$.

Here T is the time ordering operator, Ψ_0 and $\Psi(t=\infty)$ are the initial and final electron wave functions, and $H(t) = H_0 + V_{\mathrm{ext}}(t)$ is the Hamiltonian of hydrogen atoms in an external field including the contributions of IR $[V_{\mathrm{IR}}(t)]$ and the XUV $[V_{\mathrm{XUV}}(t)]$ fields, with H_0 being the external-field-free hydrogen Hamiltonian

$$H_0 = -\frac{\nabla^2}{2} - \frac{1}{r} \tag{2}$$

and

$$V_{\mathrm{ext}}(t) = \begin{cases} \mathbf{r}\cdot\mathbf{E}(t) & \text{(length gauge)} \\ \mathbf{p}\cdot\mathbf{A}(t) + \frac{A^2(t)}{2} & \text{(velocity gauge)} \end{cases} \tag{3}$$

the atom-laser interaction. The vector potential of the XUV is written as

$$\mathbf{A}_x(t) = \frac{\mathbf{E}_x}{\omega_x} e^{-t^2/\tau_x 2\ln 2} \sin(\omega_x t), \tag{4}$$

where $\mathbf{E}_x$, ω_x, and τ_x are the XUV electric-field strength, center photon energy, and pulse duration of the full width at half maximum, respectively. Similarly, the vector potential of the IR laser is written as

$$\mathbf{A}_{\mathrm{IR}}(t) = \frac{\mathbf{E}_0}{\omega} e^{-(t+t_d)^2/\tau^2 2\ln 2} \sin[\omega(t+t_d)+\delta], \tag{5}$$

where $\mathbf{E}_0$, ω, τ, and δ are the electric-field strength, photon energy, pulse duration, and the carrier-envelope phase (CEP) of the IR pulse, respectively; t_d is the time delay between the two pulses and a positive t_d means that the IR pulse arrives earlier. The total vector potential $\mathbf{A}(t) = \mathbf{A}_x(t) + \mathbf{A}_{\mathrm{IR}}(t)$ and the corresponding electric field is

$$\mathbf{E}(t) = -\frac{d\mathbf{A}(t)}{dt}. \tag{6}$$

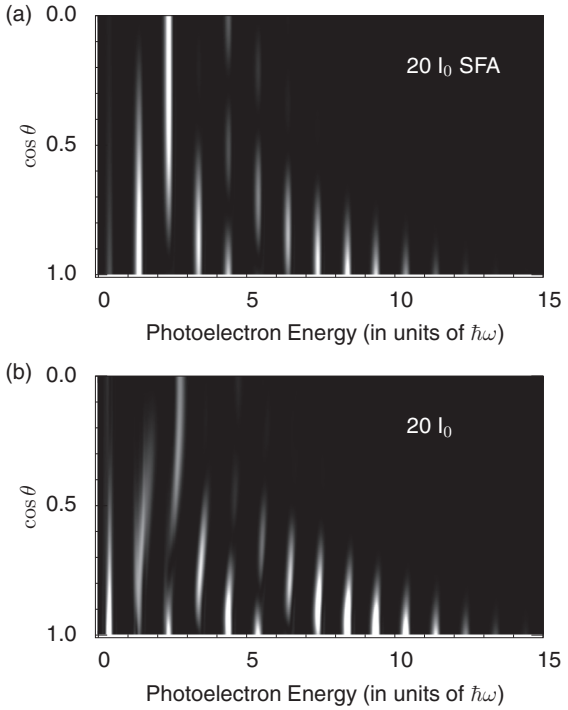

FIG. 2. Photoelectron energy-angle distribution of H atoms ionized by the XUV light in an IR field calculated by (a) the SFA (replot of Fig. 1) and (b) the TDSE for an IR intensity of $20I_0$.

If we ignore the electron nucleus Coulomb interaction in the Hamiltonian H [see Eq. (1)] in the velocity gauge [as shown in Eq. (3)], Eq. (1) goes to the SFA. In the following simulations, we assumed that the polarizations of the XUV and IR fields are parallel to each other as used in the experiments [20,21] and we set the polarization direction as the z direction.

III. RESULTS AND DISCUSSION

In this section we mainly discuss the photoelectron angular distribution of H atoms ionized by an XUV light with $\omega_x =$ 20 eV photon energy and $\tau_x = 8$ fs pulse duration in an IR field with 800-nm wavelength and $\tau = 30$ fs pulse duration. In the simulation we set the XUV intensity to $10^{11}\,\mathrm{W/cm^2}$, so the high-order effect of XUV light is negligibly small and the IR intensity is less than $50I_0$, with $I_0 = 10^{12}\,\mathrm{W/cm^2}$, so the direct ionization by the IR laser is eliminated. We also present the results with other XUV and IR parameters to show how the bending depends on the XUV and IR laser parameters. Since we focused on the photoelectron angular distribution, we plotted the photoelectron yield as a function of the electron energy and the angle of the momentum to the z direction instead of the momentum distribution as shown in Fig. 1.

A. Results of SFA and TDSE

Figure 2 shows the typical photoelectron energy-angle distributions obtained by the SFA [Fig. 2(a)] and TDSE [Fig. 2(b)] simulations with an IR intensity of $20I_0$. In the figure the SFA predicts straight-line distributions or isoenergy distributions [Fig. 2(a)], while the TDSE shows that the sideband angular distributions in the energy-angle plots bend to

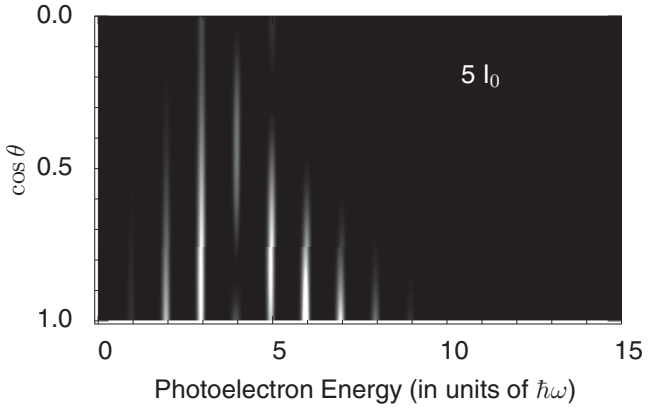

FIG. 3. Photoelectron energy-angle distribution of H atoms ionized by the XUV light in a weak IR intensity of $5I_0$.

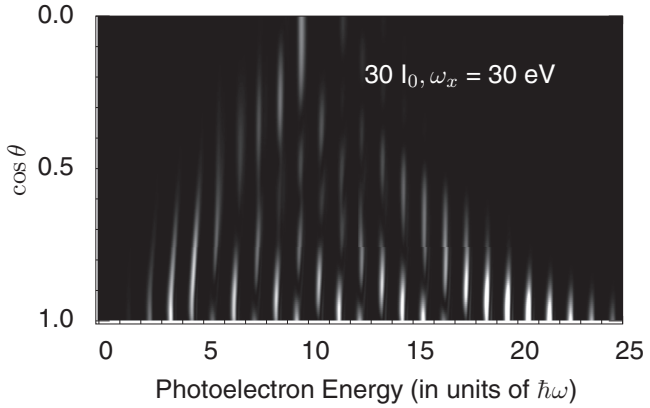

FIG. 4. Photoelectron energy-angle distribution of H atoms ionized by 30-eV XUV light in an IR laser with an intensity of $30I_0$.

higher energies for larger angles, especially for lower-energy sidebands [Fig. 2(b)]. Since the SFA ignores the Coulomb interaction after the electron is released by the XUV, the bending must be related to the electron nucleus Coulomb interaction. Without IR fields, the photoelectron shows straight-line distributions, so the bending is also coupled to the pulsed IR field. Since the bending depends on the XUV and IR laser parameters, we will investigate how the parameters affect the angular distributions.

B. IR laser intensity

Since the IR intensity is a key quantity in the strong-field material interaction, we first investigate how the intensity affects the angular distribution. For such a purpose, we analyze systematically the angular distributions from no IR laser to a relative strong one at $50I_0$ with a 10^{12}-W/cm^2 intensity step as shown in Ref. [29]. We find that with a weak IR intensity (less than 10^{13} W/cm^2), there is no visible bend as shown in Fig. 3, a typical example. As the IR intensity increases, the visible bending appears at 1.5×10^{13} W/cm^2 and the bending persists to high IR intensities. This means that both the Coulomb effect and IR laser field contribute to the bending. The incline of low-energy sidebands increases as the IR intensity increases (see movie 1 in [29]).

C. XUV photon energy

Since the Coulomb interaction is important for low-energy electrons, if we use a high-energy XUV photon, does the bending still exist? To answer the question, we increase the XUV photon energy to 30 eV as shown in Fig. 4 and find that the sidebands still bend toward high energy for large angles but the incline is smaller than the case for 20 eV with the same IR intensity. Since the visible bending starts at a high IR intensity for high XUV photon energy we show the results with a high IR intensity of $30I_0$ at which the sidebands spread more broadly and extend to the ionization threshold.

D. IR pulse duration

The atomic photoionization by an XUV light in an IR field can be explained by the Floquet theorem [8,11] and the sideband should be an isoenergy distribution or straight lines in the energy-angle plots if the IR pulse is infinitely long. If we increase the IR pulse duration to 60 fs, the bending does disappear gradually as show in Fig. 5 apart from a few lines in the very low energies; this observation is consistent with the prediction by the Floquet theorem. From this comparison, we conclude that the bending can be further originate from the phase of the photoelectron obtained in one IR cycle in a Coulomb field. The phase also depends on the direction in which the photoelectron moves. For a very long IR pulse, the obtained phase will be repeated every IR cycle, while for a short pulse, such a phase differs slightly in each IR cycle, so the final photoelectron energy depends on the direction in which the electron moves, which results in the bending. The systematic evolution of the photoelectron energy-angle distribution as a function of the pulse durations from 20 to 120 fs with a 2-fs step can be found in Ref. [29] (movie 2).

E. Time delay

Figure 6 shows that the energy-angle distribution for the IR pulse arrives 16 fs before the XUV pulse. The bending still exists, but the sidebands bend toward lower energy for large angles, which differs from the results when the two pulses overlap with each other. The systematic evolution of

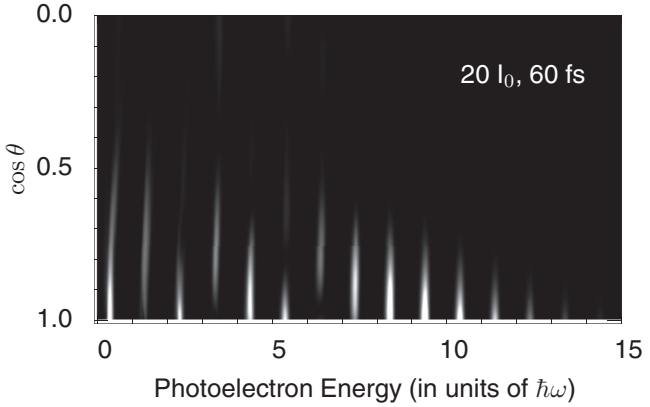

FIG. 5. Photoelectron energy-angle distribution of H atoms ionized by the XUV light in the IR field with a pulse duration of 60 fs.

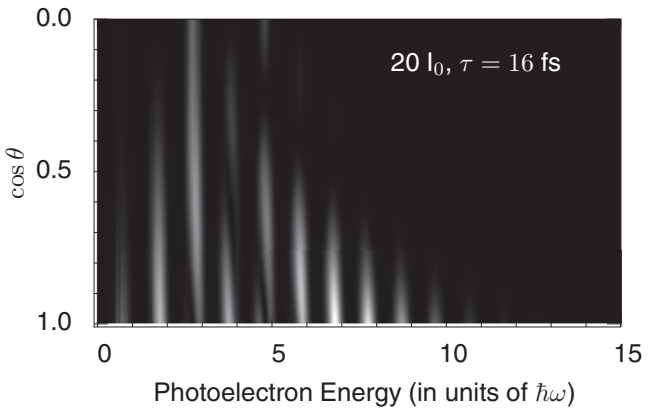

FIG. 6. Photoelectron energy-angle distribution of H atoms ionized by the XUV light in the IR field with a 16-fs time delay.

the photoelectron energy-angle distribution as a function of the time delay from −25 to 25 fs with a 1-fs step can be found in Ref. [29] (movie 3).

We see in Eq. (5) that the IR vector potential also depends on the CEP, but the TDSE results show that the bending is insensitive to the CEP. We give the conclusion here, but no longer explicate the results.

F. Physical origin

Comparing the results of the SFA and TDSE, we can identify that the Coulomb interaction results in the abnormality. We may ask why the sideband energy depends on the outgoing photoelectron direction. This is related to the phase of the photoelectron gained in the IR field after the electron is ejected from the parent atom by the XUV light. The phase is expressed as

$$\delta_p(t) = \int_t^\infty H(t')dt', \tag{7}$$

as shown in Eq. (1). If the IR pulse is infinitely long, the phase is a periodic function of time and the sidebands are always straight lines on the energy-angle plots, which do not rely on whether the Coulomb interaction is considered. If the IR pulse is not infinitely long, the phase obtained within each IR cycle differs slightly since the detailed IR electric field changes cycle by cycle, so the sidebands are almost on the isoenergy rings if the Coulomb interaction is ignored. If the Coulomb interaction is considered, the phase of the photoelectron moving in a Coulomb field within one IR cycle depends on the electron trajectory or the direction of movement. Since the Coulomb effect is important for low-energy electrons, the inclines are larger for lower-energy sidebands. The detailed dependence could be complex, but the physical explanation should be right from the above discussion. We also calculated the photoelectron angular distribution by replacing the XUV light from the free-electron laser with the APT and the bending still exists.

This observation is related to the ionization surprise, which was observed in above-threshold ionization (ATI) in experiments [30,31] and attributed the surprise to the photoelectron Coulomb interaction [32–35]. If we carefully look at the two-dimensional momentum distributions of the photoelectron in intense mid-IR laser fields [36–39], indeed the photoelectrons are not isoenergetically distributed, especially on the low-energy side. Therefore, even for the atomic ATI spectra in an intense IR field, the SFA does not work very well for the angular distribution of low-energy ATIs.

The mechanism of bending of the photoelectron angular distribution for an IR-assisted photoionization in a long XUV pulse is different from the one for an IR-assisted SAP photoionization. For the SAP, the energy spreads broadly and covers several IR photon energies, so there are no sidebands clearly separated by one IR photon energy. The SAP can be used for the streaking experiments [40–43].

IV. CONCLUSION

In this work we have investigated the bending of the photoelectron angular distribution of atoms ionized by an XUV light assisted by a moderately intense IR laser field. The bending is attributed to the photoelectron nucleus Coulomb interaction since the angular distribution returns to a straight line in the energy-angle plots if the Coulomb interaction is ignored in the simulation. The bending depends on the XUV photon energy, IR intensity, IR pulse duration, and time delay between the two pulses. Therefore, it can be used to calibrate or obtain the laser parameters by comparing measurements with simulations. Note that the focal volume averaging is not important since the focal size of XUV sources, like APT, is much narrower than the focal size of IR fields. The effect is also not sensitive to the atomic species since the XUV creates a quasifree electron and the IR electric field causes the quasifree electron to change its momentum.

ACKNOWLEDGMENTS

This work was supported by a Grant-in-Aid for Scientific Research (Grant No. JP16K05495) from the Japan Society for the Promotion of Science. The TDSE calculations were performed using Oakforest-Pacs at Center for Computational Sciences, University of Tsukuba.

[1] X. F. Li, A. L'Huillier, M. Ferray, L. A. Lompre, and G. Mainfray, Phys. Rev. A **39**, 5751 (1989).
[2] A. L'Huillier, K. J. Schafer, and K. C. Kulander, J. Phys. B **24**, 3315 (1991).
[3] V. Véniard, R. Taïeb, and A. Maquet, Phys. Rev. Lett. **74**, 4161 (1995).
[4] T. E. Glover, R. W. Schoenlein, A. H. Chin, and C. V. Shank, Phys. Rev. Lett. **76**, 2468 (1996).
[5] E. S. Toma, H. G. Muller, P. M. Paul, P. Breger, M. Cheret, P. Agostini, C. Le Blanc, G. Mullot, and G. Cheriaux, Phys. Rev. A **62**, 061801(R) (2000).

[6] P. Johnsson, J. Mauritsson, T. Remetter, A. L'Huillier, and K. J. Schafer, Phys. Rev. Lett. **99**, 233001 (2007).

[7] P. Ranitovic, X. M. Tong, B. Gramkow, S. De, B. DePaola, K. P. Singh, W. Cao, M. Magrakvelidze, D. Ray, I. Bocharova, H. Mashiko, A. Sandhu, E. Gagnon, M. M. Murnane, H. Kapteyn, I. Litvinyuk, and C. L. Cocke, New J. Phys. **12**, 013008 (2010).

[8] S.-I. Chu and D. A. Telnov, Phys. Rep. **390**, 1 (2004).

[9] X. M. Tong, P. Ranitovic, C. L. Cocke, and N. Toshima, Phys. Rev. A **81**, 021404(R) (2010).

[10] X.-M. Tong and N. Toshima, Phys. Rev. A **81**, 043429 (2010).

[11] X. M. Tong and N. Toshima, Phys. Rev. A **81**, 063403 (2010).

[12] P. Ranitovic, X. M. Tong, C. W. Hogle, X. Zhou, Y. Liu, N. Toshima, M. M. Murnane, and H. C. Kapteyn, Phys. Rev. Lett. **106**, 193008 (2011).

[13] P. Antoine, A. L'Huillier, and M. Lewenstein, Phys. Rev. Lett. **77**, 1234 (1996).

[14] P. M. Paul, E. S. Toma, P. Breger, G. Mullot, F. Auge, P. Balcou, H. G. Muller, and P. Agostini, Science **292**, 1689 (2001).

[15] Z. Chang, Phys. Rev. A **70**, 043802 (2004).

[16] G. Sansone, E. Benedetti, F. Calegari, C. Vozzi, L. Avaldi, R. Flammini, L. Poletto, P. Villoresi, C. Altucci, R. Velotta, S. Stagira, S. De Silvestri, and M. Nisoli, Science **314**, 443 (2006).

[17] Z. Huang and K.-J. Kim, Phys. Rev. ST Accel. Beams **10**, 034801 (2007).

[18] A. Cionga, V. Florescu, A. Maquet, and R. Taieb, Phys. Rev. A **47**, 1830 (1993).

[19] A. K. Kazansky, I. P. Sazhina, and N. M. Kabachnik, Phys. Rev. A **82**, 033420 (2010).

[20] S. Minemoto, H. Shimada, K. Komatsu, W. Komatsubara, T. Majima, T. Mizuno, S. Owada, H. Sakai, T. Togashi, S. Yoshida, M. Yabashi, and A. Yagishita, J. Phys. B **51**, 075601 (2018).

[21] J. Hummert, M. Kubin, S. D. López, M. J. J. Vrakking, O. Kornilov, and D. G. Arbó, arXiv:1808.04639.

[22] M. Lewenstein, P. Balcou, M. Y. Ivanov, A. L'Huillier, and P. B. Corkum, Phys. Rev. A **49**, 2117 (1994).

[23] A. L'Huillier, M. Lewenstein, P. Salières, P. Balcou, M. Y. Ivanov, J. Larsson, and C. G. Wahlström, Phys. Rev. A **48**, R3433(R) (1993).

[24] A. Becker and F. H. M. Faisal, J. Phys. B **38**, R1 (2005).

[25] A.-T. Le, H. Wei, C. Jin, and C. D. Lin, J. Phys. B **49**, 053001 (2016).

[26] X.-M. Tong and S.-I. Chu, Chem. Phys. **217**, 119 (1997).

[27] X. M. Tong, K. Hino, and N. Toshima, Phys. Rev. A **74**, 031405(R) (2006).

[28] X. M. Tong, S. Watahiki, K. Hino, and N. Toshima, Phys. Rev. Lett. **99**, 093001 (2007).

[29] See Supplemental Material at http://link.aps.org/supplemental/10.1103/PhysRevA.99.043422 for the photoelectron angular distribution of hydrogen atoms ionized by an XUV light in the IR fields with different IR intensities (movie 1), different IR pulse durations (movie 2), and different time delays between the two pulses (movie 3).

[30] C. I. Blaga, F. Catoire, P. Colosimo, G. G. Paulus, H. G. Muller, P. Agostini, and L. F. DiMauro, Nat. Phys. **5**, 335 (2009).

[31] W. Quan, Z. Lin, M. Wu, H. Kang, H. Liu, X. Liu, J. Chen, J. Liu, X. T. He, S. G. Chen, H. Xiong, L. Guo, H. Xu, Y. Fu, Y. Cheng, and Z. Z. Xu, Phys. Rev. Lett. **103**, 093001 (2009).

[32] F. H. M. Faisal, Nat. Phys. **5**, 319 (2009).

[33] C. Liu and K. Z. Hatsagortsyan, Phys. Rev. Lett. **105**, 113003 (2010).

[34] T.-M. Yan, S. V. Popruzhenko, M. J. J. Vrakking, and D. Bauer, Phys. Rev. Lett. **105**, 253002 (2010).

[35] L. Guo, S. S. Han, X. Liu, Y. Cheng, Z. Z. Xu, J. Fan, J. Chen, S. G. Chen, W. Becker, C. I. Blaga, A. D. DiChiara, E. Sistrunk, P. Agostini, and L. F. DiMauro, Phys. Rev. Lett. **110**, 013001 (2013).

[36] Y. Huismans, A. Rouzée, A. Gijsbertsen, J. H. Jungmann, A. S. Smolkowska, P. S. W. M. Logman, F. Lépine, C. Cauchy, S. Zamith, T. Marchenko *et al.*, Science **331**, 61 (2011).

[37] D. D. Hickstein, P. Ranitovic, S. Witte, X.-M. Tong, Y. Huismans, P. Arpin, X. Zhou, K. E. Keister, C. W. Hogle, B. Zhang, C. Ding, P. Johnsson, N. Toshima, M. J. J. Vrakking, M. M. Murnane, and H. C. Kapteyn, Phys. Rev. Lett. **109**, 073004 (2012).

[38] C. Lemell, K. I. Dimitriou, X.-M. Tong, S. Nagele, D. V. Kartashov, J. Burgdörfer, and S. Gräfe, Phys. Rev. A **85**, 011403(R) (2012).

[39] X.-M. Tong, P. Ranitovic, D. D. Hickstein, M. M. Murnane, H. C. Kapteyn, and N. Toshima, Phys. Rev. A **88**, 013410 (2013).

[40] J. Itatani, F. Quéré, G. L. Yudin, M. Y. Ivanov, F. Krausz, and P. B. Corkum, Phys. Rev. Lett. **88**, 173903 (2002).

[41] E. Goulielmakis, M. Uiberacker, R. Kienberger, A. Baltuska, V. Yakovlev, A. Scrinzi, T. Westerwalbesloh, U. Kleineberg, U. Heinzmann, M. Drescher, and F. Krausz, Science **305**, 1267 (2004).

[42] M.-H. Xu, L.-Y. Peng, Z. Zhang, Q. Gong, X.-M. Tong, E. A. Pronin, and A. F. Starace, Phys. Rev. Lett. **107**, 183001 (2011).

[43] M. Kübel, Z. Dube, A. Y. Naumov, M. Spanner, G. G. Paulus, M. F. Kling, D. M. Villeneuve, P. B. Corkum, and A. Staudte, Phys. Rev. Lett. **119**, 183201 (2017).